Sputtered SnTe thin films on Si and Ge as a plasmonic material

Tri Nguyen[1], Leland Nordin[2], Kunal Mukherjee[1]*

[1]Materials Science and Engineering, Stanford University, CA 94305, United States

[2]Geballe Laboratory for Advanced Materials, Stanford University, CA 94305, United States

ABSTRACT: We demonstrate the potential of SnTe films as a mid-infrared plasmonic material, harnessing its innate ability to be degenerately p-type doped above $10^{20}/cm^3$. SnTe, a narrow bandgap rocksalt semiconductor, is deposited on CMOS-compatible substrates of Si (001) and Ge (001) using sputtering as a scalable deposition method. We identify a growth window for sputtering SnTe films and find that films on Ge substrates have grains with defined epitaxial relationships to the substrate and lower surface roughness compared to largely polycrystalline grains on Si. Despite differences in crystallinity in SnTe across these two substrates, we find similar scattering losses at optical wavelengths that is comparable to other high quality semiconductors, and this is mirrored in our finding that electrical transport in our polycrystalline films is as much as half that of high-quality bulk crystals. Finally, we show that changing the growth temperature tunes the plasma wavelength of our material across 3.9 – 5.3 μm, likely by altering the Sn/Te stoichiometry and provides supplementary methods to extrinsic dopants.

KEYWORDS: SnTe, plasmonics, sputtering, heteroepitaxy, semiconductors

*kunalm@stanford.edu

INTRODUCTION

Plasmonic and metamaterial structures attract significant interest for applications in sensing and waveguiding.[1–4] While plasmonic structures traditionally utilize noble metals, doped semiconductors also have shown great promise as tunable plasmonic materials especially in the mid-infrared (mid-IR).[5–14] One of the key advantages of doped semiconductors is the ease of seamless epitaxial integration with active devices such as emitters and detectors, not feasible with noble metals. Group IV semiconductors like Ge and III-V semiconductors like InAs – and ternary alloys InGaAs, InAsSb – stand out as excellent mid-IR plasmonic materials with high maximum doping level, small carrier effective mass, and a broad tunability of plasma wavelength.[5,6,8,9,15,16] The synthesis of III-V semiconductors with excellent optical properties and low carrier scattering loss, however, requires ultra-high-vacuum (UHV) techniques such as molecular beam epitaxy (MBE) and thus severely limits scalability and hinders widespread applications. Hence, there is a need to identify a highly doped semiconductor that can offer performance comparable to MBE plasmonic materials, but with a more cost-effective and scalable synthesis route and without adversely affecting scattering losses. Additionally, this material should be compatible for integration with CMOS processes and substrates like Si and Ge. Most importantly, it must maintain a tunable plasma wavelength in the mid-IR through carrier concentration control.

Tin telluride (SnTe), a IV-VI narrow-bandgap semiconductor (E_g = 0.18 eV at 300K[17]), is a promising plasmonic mid-IR material that can be easily synthesized using cost-effective sputtering techniques, integrated in CMOS processes, and possesses a tunable plasma wavelength. Specifically, SnTe can be sputtered from a compound target as the

vapor pressures of Sn and Te are not as dissimilar as group-III and group-V elements. It has a cubic rocksalt crystal structure making it compatible with cubic semiconductors for epitaxial integration. Finally, SnTe has a very high maximum hole doping limit set by a Fermi energy stabilization point deep in the valence band.[18] Even in the absence of extrinsic p-type dopants, SnTe naturally favors being Sn-deficient.[18,19] The Sn deficiency manifests as negatively charged Sn vacancies which results in hole concentrations on the order of 10^{20} – 10^{21} cm^{-3}. Such a high concentration of holes leads to high free carrier reflection of SnTe in the 3-8 μm wavelengths.[20–23]

There are preliminary indications that sputtering can be used to realize SnTe films as a good plasmonic material on technologically relevant substrates if a few obstacles are overcome. Epitaxial films of sputtered SnTe have been reported on NaCl substrates[24], but sputtered growth of SnTe films on MgO[25] and CMOS-compatible substrates of Si and Ge[24,26,27] has so far yielded polycrystalline films. It is important to understand whether polycrystalline growth is inevitable or if single crystal growth is possible on these CMOS-compatible substrates, given that SnTe (a = 6.32 Å) has a relatively large lattice mismatch of 16.4% on Si (a = 5.43 Å) and 11.6% on Ge (a = 5.66 Å), respectively. At the same time, while carrier concentration control via nonstoichiometry is widely explored in SnTe bulk crystals with equilibrium thermal annealing under excess Sn or Te conditions, there has not been a systematic study under nonequilibrium sputtering conditions. Understanding this intrinsic control of carrier concentration serves as a precursor to future work with extrinsic dopants. In addition to tuning the free carrier concentration, it is important to quantify carrier scattering rates at optical wavelengths in sputtered SnTe that results in loss and compare it to high quality bulk crystals. Traditionally, in III-V semiconductors, there

is a notion that achieving good crystal quality is key to low loss plasmonic materials, particularly in ultra-high doped films where the extreme dopant fluxes may be disruptive to epitaxial growth.[15,16] It is therefore interesting to ask if carrier scattering rates in SnTe are as sensitive to crystal quality, especially since we expect that sputtered films on highly mismatched Si and Ge are going to be of lower quality than those made by UHV methods.

METHODS

SnTe films with thicknesses in the range 60 – 350 nm were grown on Si (001) and Ge (001) substrates using a Kurt J. Lesker magnetron sputter deposition system with a base pressure of ~1.5×10^{-7} Torr. The sputter deposition system is equipped with both RF and DC magnetron sputtering sources. Traditionally, RF sputtering is recommended for depositing semiconductors including SnTe, since most semiconductors are not as conductive as metals. However, DC sputtering source was found to be capable of depositing SnTe thin films (see supplementary material Figure S1). We suspect this is due to the low resistivity of SnTe of ~1.8×10^{-6} Ω-m, which is comparable to that of metals. While the versatility of SnTe to be sputtered using either DC or RF source is exciting, we mainly focus on SnTe films grown using RF source in this study. Prior to deposition, the SnTe compound target was sputter-etched for 15 min with a shutter shielding the substrate. During the film growth, the flow rate of Ar gas was fixed to be 50 sccm and the sputter gas pressure was 3 mTorr. SnTe films were deposited at 60 W RF power, corresponding to a relatively slow growth rate of ~2.5 – 3 nm/min. Substrate temperature was varied in the range of 20 – 300 °C during the study. We primarily focus on the 350 nm samples for structural and optical characterization, as these films are optically thick. On the other hand, we use the thin 60 nm and 100 nm films to understand the transport properties of sputtered

SnTe films. Finally, we compare the effectiveness of native oxide removal between wet and in-situ etching.

We started with commercially available high resistivity Si (001) substrates. Prior to growth, the Si (001) substrates were cleaned in ultrasonic baths of acetone, methanol, and isopropyl alcohol to remove dust and to degrease, followed by blowing dry with N_2. Two surface treatments to remove the native oxide of Si were investigated: in-situ etching using Ar gas inside the sputtering chamber, and ex-situ wet etching using hydrofluoric acid (HF).

For in-situ removal of the native oxide, the Si substrate was Ar etched for five minutes at 40W RF power before deposition at a chamber pressure of 3 mTorr. For wet etching of the native oxide, the substrates were dipped into 2% HF for two minutes. After the HF treatment, the substrates were rinsed in de-ionized water and blown dry with N_2. Right after this step, the substrates were quickly transferred to the sputtering chamber.

In addition to Si substrates, we explored Ge substrates for heteroepitaxial growth of SnTe films. Ge substrates of (001) orientation (University Wafer) were cleaned in situ prior to deposition. The substrates were heated to 650 °C for an hour to thermally desorb the oxide. The temperature was ramped down at 20 °C/minute to the deposition temperature. We did not attempt to compare this to Ar-sputtering removal of the native Ge oxides.

The crystal structure and quality of as-grown SnTe films was examined by high-resolution x-ray diffraction (HRXRD) using a Panalytical X-Pert PRO MRD system with Cu-$K\alpha_1$ source. Atomic force microscopy (AFM) images were acquired with non-tapping mode on a Park NX-10 to characterize the surface topography and measure the surface roughness of SnTe films. Hall carrier concentration and mobility at room temperature was

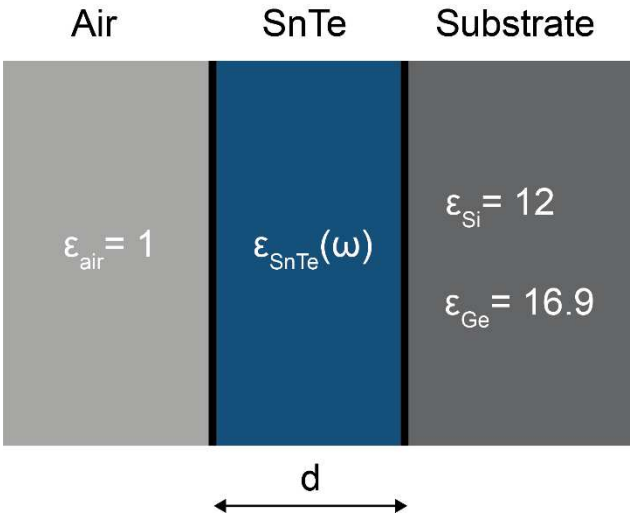

Figure 1. *Schematic of a 3-layered transfer matrix used in the fitting model, including air, SnTe thin film, and substrate. The dielectric function of the SnTe layer is modeled as a Drude metal as described in equation (1).*

measured on a Lakeshore 8404 Hall using a four-point van der Pauw configuration with pressed indium dots as contacts.

Optical characterization in the 1.5 – 15 μm range was performed with a Nicolet iS50 Fourier transform infrared (FTIR) spectrometer equipped with a VeeMax specular reflectance accessory. We collected the reflection spectra at 30º incident angle using a DTGS KBr detector with a spectral resolution of 4 cm^{-1}. All the reflection data were normalized to an optically thick layer of evaporated gold that has a reflection close to unity in the mid-IR. For the reflection modeling, we used the transfer matrix (T-matrix) method to fit the experimental reflection data of each sample. Figure 1 shows a three-layered structure used in the model, including the air, the SnTe film, and the substrate.

The air and the substrate are assumed to be infinitely thick. The reflection of SnTe was modeled as a Drude metal with contributions from conduction holes as free carriers:

$$\epsilon = \epsilon_{opt}\left(1 - \frac{\omega_p^2}{\omega^2 + i\omega\gamma}\right) \quad (1)$$

where ϵ_{opt} is the background permittivity, which is fixed to be 40 for SnTe films[28] in this work. Together with the SnTe layer thickness (d), we iteratively fit the plasma frequency, ω_p, the scattering rate of the carriers γ. The thickness was fitted to be around ~350 nm for SnTe thin films used for the structural and optical characterization. While the narrow bandgap of SnTe of ~0.2 eV could introduce bound-carrier absorption effect that is not accounted for in the free carrier dispersion theory at wavelengths shorter than ~6 μm, the bound-carrier extinction coefficient turns out to be negligible for the high hole concentration greater than ~10^{20} cm^{-3} of the deposited SnTe films due to the Burstein-Moss effect.[21] The higher the hole concentration, the deeper the Fermi level extends through the valence band, effectively increasing the band gap of SnTe and shifting the onset of the bound-carrier absorption to wavelengths less than ~3 μm. Since this wavelength is almost outside of the fitting regime, we assume the bound-carrier absorption effect to be negligible in the fitting model.

RESULTS AND DISCUSSION

Sputtered SnTe on Si (001)

In line with previous work, we are unable to obtain epitaxial growth of SnTe on Si via sputtering over a range of conditions.[24,27] We speculate, largely informed by extensive work on III-V-on-Si integration, that SnTe growth on Si requires high temperature substrate bakes (in excess of 1100 °C for UHV[29] and 800 °C under H_2 ambient[30]) to achieve a good surface step structure after removal of the native oxide. While this is not possible via in a conventional sputtering chamber, the SnTe films on Si are an excellent candidate

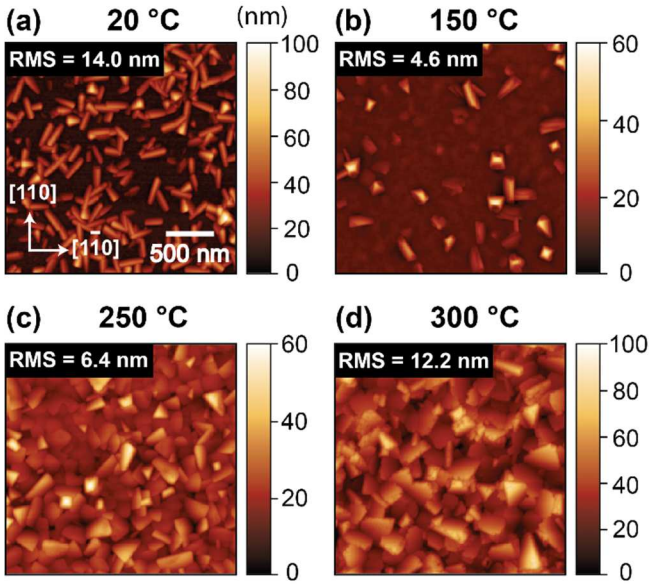

Figure 2. *AFM topography maps of SnTe films on Si (001) deposited at (a) 20 ℃, (b) 150 ℃, (c) 250 ℃, and (d) 300 ℃. The scan area is 2.5 x 2.5 μm^2.*

to understand the relationship between SnTe film crystallinity, sputtering conditions, carrier concentration, and the plasmonic properties of the SnTe films.

We first explore the effect of substrate temperature on the structural properties of SnTe films, maintaining a sputter pressure of 3 mTorr and a deposition power of 60 W. Figure 2 shows AFM scans of the morphology of non-epitaxial films for all the temperatures investigated. The native oxides of Si were removed by HF treatment. At 20 ℃, the film structure displays clusters of island-like features at random orientations and a high RMS roughness of 14 nm (Fig. 2a). As the substrate temperature is increased to 150 ℃, which increases the mobility of the adatoms, the RMS roughness decreases to 4.6 nm but some faceted grain structure is still present on the surface (Fig. 2b). For the SnTe films grown at 250 ℃ and 300 ℃, the faceted structure increases in prominence, reflected also in an increase in the RMS roughness to 6.4 and 12.2 nm respectively (Fig. 2c-d).

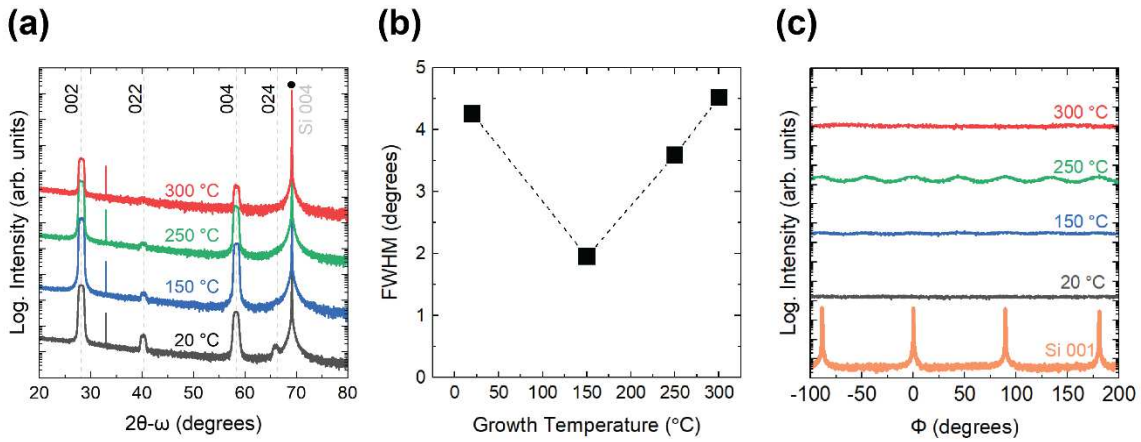

Figure 3. *(a) Symmetric 2θ/ω scans of SnTe films on Si (001). (b) Symmetric (002) rocking curve FWHM versus growth temperature. (c) 360º phi scans of SnTe (001) films deposited at different growth temperatures, showing SnTe and Si {224}at χ = 35.26º.*

To evaluate film crystallinity across the growth temperature series, we performed x-ray diffraction measurements. Figure 3a shows a symmetric 2θ/ω XRD scans of the SnTe/Si(001) films. We find (00*l*)-type out-of-plane reflections are prominent in the SnTe films, even at room temperature. Indeed, the nonpolar (002) planes have the lowest surface energy in SnTe. As the growth temperature increases, the intensity of the minority SnTe (022) out-of-plane grains decreases but cannot be suppressed completely. We perform 360º φ-scans in skew-symmetric geometry on the {224} peaks of only the majority (002) out-of-plane SnTe grains to see if there is an in-plane epitaxial relationship. Figure 3c clearly shows that a four-fold symmetry corresponding to cube-on-cube epitaxy is not present for SnTe films deposited at 20 °C, 150 °C, and 300 °C, indicating randomly oriented polycrystalline films (specifically a fiber-texture). For the film grown at 250 °C, the φ-scan reveals hints of two domains: unrotated cube-on-cube epitaxy and a 45º–rotated crystal in the substrate azimuthal orientation, but it is not possible to estimate the volume fraction these grains. Overall, our experiments show that further surface treatment is necessary to

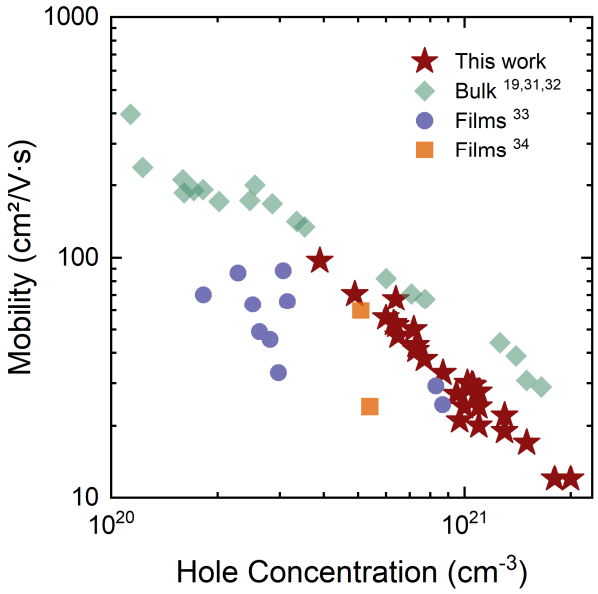

Figure 4. *Hall carrier density and apparent hole concentration of SnTe (red stars) at room temperature. Literature values for bulk films*[19,31,32] *and thin films*[33,34] *are also plotted for comparison.*

understand how to nucleate an epitaxial SnTe film directly on Si. Nevertheless, these films serve as a good benchmark to test the limits of crystallinity on plasmonic properties.

To understand the relationship between sputtering conditions and transport properties, we perform Hall effect measurements on the polycrystalline SnTe films on Si. The measurements show not only that the hole concentration can be slightly tuned with the growth conditions, but also that the carrier mobility remains comparable to high quality bulk crystals. Figure 4 shows this trend measured across synthesis conditions (growth temperature, film thickness, Ar-etch or HF native oxide removal, and pre-deposition substrate bake). The electrical properties are predominantly controlled by growth temperature. We do not notice any significant difference in transport properties between the cases of Ar-etched and HF-etched silicon oxide removal, which we believe strongly suggests the need for a high temperature bake before SnTe film growth.

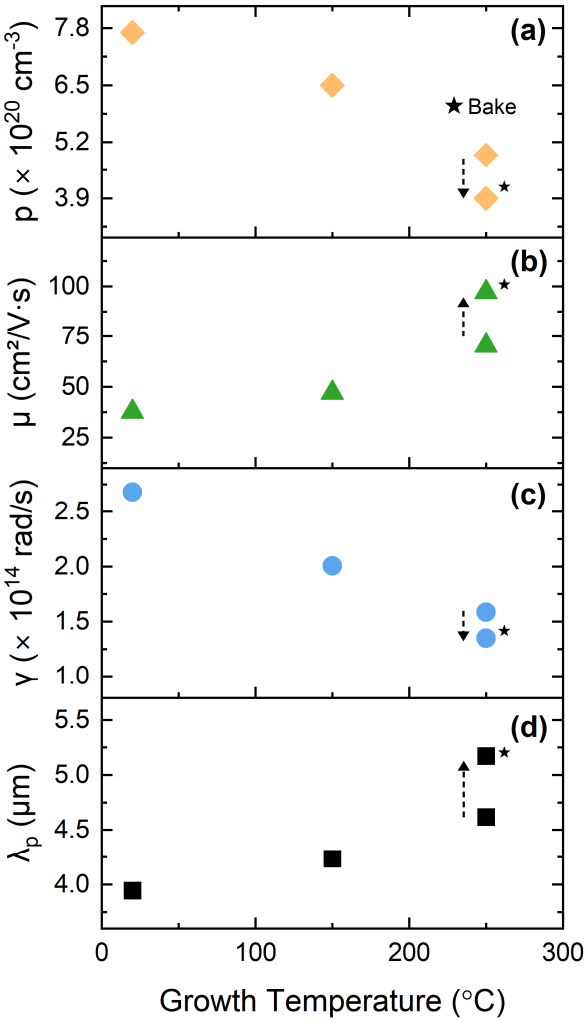

Figure 5. *Hole concentration (a) and mobility (b) as extracted from Hall measurements and scattering rate (c) and plasma wavelength (d) as determined from optical measurements and modelling as a function of growth temperature for SnTe films grown on Si (001) substrate. The SnTe/Si(001) film deposited at 250 °C that was subject to the pre-deposition substrate bake at 650 °C for 1 hour is indicated by the stars.*

For the case of silicon native oxide removal by HF, we find that as growth temperature increases from 20 °C to 250 °C, the hole concentration reduces from 7.7 × 10^{20} to 4.9 × 10^{20} cm^{-3} with an accompanying increase in hole mobility from 38 to 70 cm^2/V-s (Fig 5a-b). Drawing on previous IV-VI results, electrical carrier concentration in undoped samples provides direct information on the stoichiometry.[19] The creation of one Sn vacancy (V_{Sn}^{2-})

corresponds to the generation of two holes (h^+). Since SnTe is intrinsically p-type due to Sn vacancies (and potentially Te-antisites), higher substrate temperature could lead to Te re-evaporation, thereby decreasing the Sn vacancies or hole concentrations and subsequently moving the stoichiometry towards unity. Similar trends were observed in MBE-grown epitaxial SnTe(001)/BaF_2(001)[35] and SnTe(111)/Sapphire(0001)[33]. An additional step of a substrate bake at 650 °C for 1 hour prior to deposition further reduces the carrier concentration to 3.9×10^{20} cm^{-3} and increases the mobility to 97 cm^2/V-s. The dominant hole scattering mechanism in electrical measurements in bulk SnTe is reported to be driven by acoustic phonons.[17,36] As the Fermi level is pushed deeper into the valence band for increased hole doping, there are more final states that holes may scatter to after interacting with the acoustic phonons, leading to the monotonic decline in hole mobility. The high dielectric constant of SnTe makes hole-hole or ionized impurity scattering negligible even at carrier concentrations of 10^{20} – 10^{21} cm^{-3}. Thus, we may expect that carrier scattering with charged crystal defects (grain boundaries, dislocations etc.) that ordinarily affect III-V semiconductors may be similarly screened in SnTe and lead to reasonable transport in polycrystalline films. We also find an effect of thicker films (350 nm vs. 60 nm) systematically reducing the doping by a factor of two (Figure S2), suggesting a potential interfacial connection to free carrier concentration, but we do not explore this further.

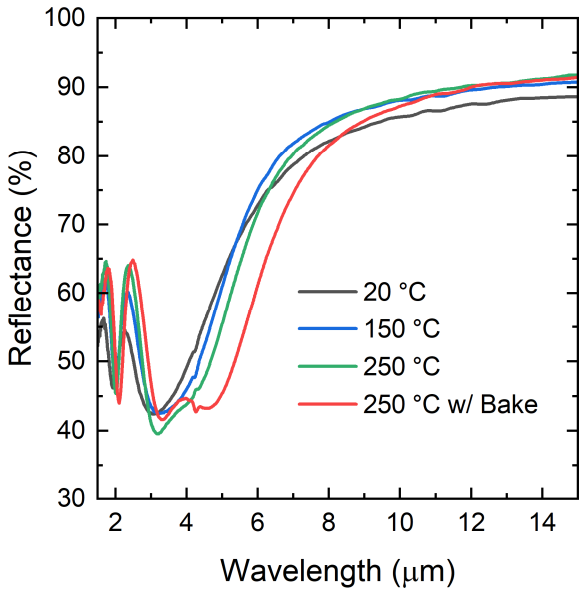

Figure 6. *Reflectance spectra of SnTe/Si(001) deposited at varying growth temperatures and conditions.*

With a degree of control over the carrier concentration via native point defects and room temperature mobilities half that of bulk crystals despite the polycrystalline nature of the films, we ask whether this trend translates also to the optical properties. Figure 6 shows the reflection spectra of a subset of the SnTe films discussed above. We find a transition from a high transmission state expected at shorter wavelengths, to a high reflection state at longer wavelengths, as the materials transition from positive to negative real permittivity. Oscillations are observed due to a Fabry-Perot cavity produced by the SnTe film and the SnTe/Si and Si/air interface. As expected, an increase in growth temperature results in a red shift of the reflection due to decreasing hole concentration. The SnTe film that underwent the 1-hour 650°C bake before deposition has a significantly redshifted Drude edge. The extracted values for carrier scattering rate γ and plasma wavelength ($\lambda_p = 2\pi c/\omega_p$) are shown in Figure 5c-d. The modeled spectra are in good agreement with the

experimental data (see supplementary Figure S4a-d). The scattering rate γ decreases as growth temperature increases, showing a decrease concomitant with the hole concentration, to the lowest value of 1.4×10^{14} rad/s for a 5.2 μm plasma wavelength. We fit the data from Bis and Dixon[20] and obtain the bulk sample scattering rate of 1.1×10^{14} rad/s for a hole concentration of 3×10^{20} cm^{-3}, which is comparable to our sputtered polycrystalline films.

To summarize, the electrical and optical properties of sputtered polycrystalline films of SnTe on Si show a degree of tunability by varying the growth temperature and thus altering the native point defects concentration. The carrier scattering rates at DC and optical frequencies remain comparable to bulk single crystals. The absence of SnTe epitaxy, likely due to improper preparation of the Si surface, suggests that device integration cannot proceed directly on Si. As described in the subsequent section, we use Ge substrates as an alternate where native oxide removal occurs at lower temperatures.

Sputtered SnTe on Ge (001)

Mirroring our investigation of sputtered SnTe on Si, we study the effect of growth temperature on epitaxial quality of SnTe films on Ge substrates. There are two key advantages in considering Ge as an alternative substrate over Si. First, single-crystal heteroepitaxial growth of IV-VI family semiconductors such as $Pb_{1-x}Sn_xTe$ and PbSe on Ge substrates have been reported.[37,38] Second, all Ge oxides can be thermally desorbed by heating to temperatures between 400 – 600 °C.[39–44] SnTe films were grown on Ge at varying growth temperatures: 20 °C, 150 °C, 250 °C, and 300 °C. The native oxides of Ge

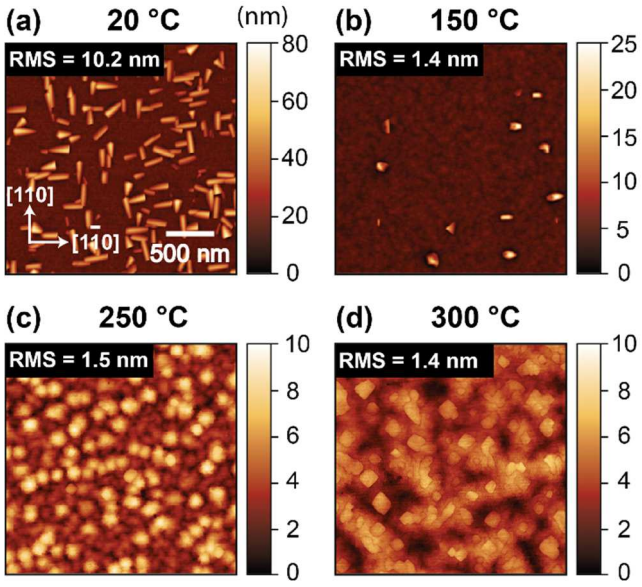

Figure 7. *AFM topography maps of SnTe films on Ge (001) deposited at (a) 20 °C, (b) 150 °C, (c) 250 °C, and (d) 300 °C. The scan area is 2.5 x 2.5 μm^2.*

were removed in-situ by baking at 650 °C for an hour under high-vacuum before deposition.

Figure 7 illustrates the effect of increasing the growth temperature on the AFM surface morphology of SnTe films. At 20 °C, the RMS is high at 10.2 nm due to several misoriented grains with prominent faceting towering above the film. As the growth temperature increases, the RMS drops significantly to 1.4 nm, but a few grains remain misoriented, with morphologies varying from triangles to rectangles. The morphology of the film in the background may be seen more clearly in S3. At 250 °C, the RMS does not change much at around 1.5 nm, while grain sizes increase and coalesces. As the temperature is increased to 300 °C, the RMS remains constant, and the surface develops a texture with diamond facets.

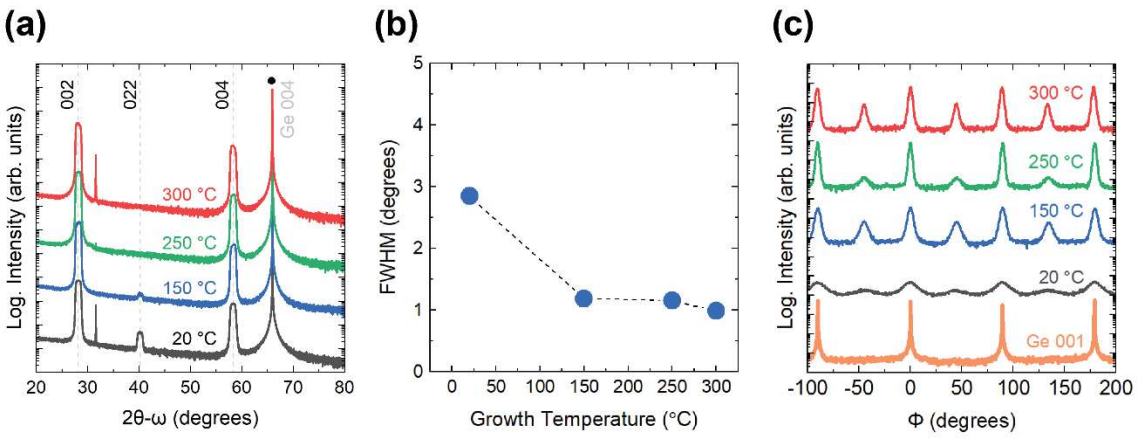

Figure 8. *(a) Symmetric 2θ/ω scans of SnTe films on Ge (001). (b) Symmetric (002) rocking curve FWHM versus growth temperature. (c) 360⁰ phi scans of SnTe (001) films showing SnTe and Ge {224}at χ = 35.26⁰.*

The significant decrease in the film roughness at higher growth temperatures corresponds to the changes in the crystal orientation and quality of SnTe films, as shown in the HR-XRD measurements. Figure 8a shows a symmetric 2θ/ω scan of the SnTe/Ge (001) films. Reflections from (002), (022), and (004) peaks were detected for SnTe films grown at room temperature and 150 ℃, indicating that these films grew multiple-orientation out-of-plane. At 250 ℃ and 300 ℃, only (00*l*)-type reflections are present, showing that these films growing single-orientation out-of-plane. Figure 8b shows the full width half maximum (FWHM) of the SnTe (002) rocking curve. As the growth temperature is increased from 20 ℃, the FWHM decreases from 2.85 degrees to 1.19 degrees, corresponding to an increase in crystal quality. As the growth temperature increases above 150 ℃, the FWHM slightly decreases to 1.16 degrees at 250 ℃ and to 0.99 degrees at 300 ℃. The FWHM follows the same trend as the RMS roughness of SnTe films deposited at 150 ℃ and above. Figure 9c shows the 360⁰ phi scans on the {224} peaks of SnTe and Ge, revealing two distinct domains: the unrotated cube-on-cube epitaxy and in-plane 45⁰ – rotated epitaxy.

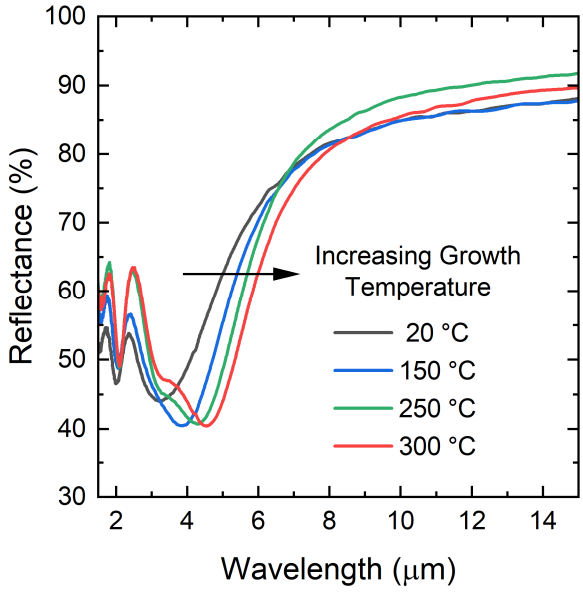

Figure 9. *Reflectance spectra of SnTe/Ge(001) deposited at varying growth temperatures.*

As the growth temperature is increased from room temperature to 250 ºC, the volume fraction of cube-on-cube epitaxial grains, judged from the peak intensity, increases monotonically from 63% to 93%. However, as the temperature is increased to 300 ºC, the cube-on-cube epitaxial volume decreases to 81%. The rotation of the grain increases the absolute value of lattice-mismatch between SnTe and Ge from 11.6% to 20.7% and hence is surprising to see at higher temperatures. To probe whether the source of the non-monotonic behavior between 250 and 300 ºC arises from the initial nucleation or the subsequent growth, we can decouple nucleation and growth (such as nucleation at 250 °C and film growth at 300 °C) in future work.

We do not report Hall-effect measurements due to the non-insulating nature of the Ge substrates and proceed directly to reflection measurements. Like on Si, Figure 9 shows that an increase in the growth temperature results in the red shift of the reflection spectra of the SnTe films grown on Ge. The values for scattering rate and plasma wavelength obtained

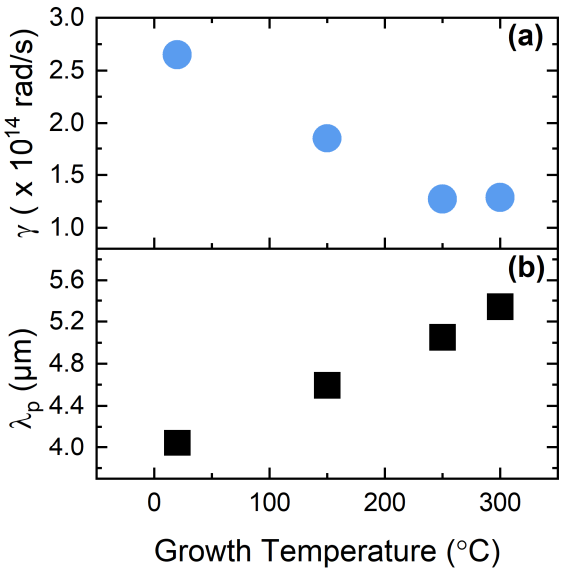

Figure 10. *Scattering rate (a) and plasma wavelength (b) as determined from optical measurements and modelling as a function of growth temperature for SnTe films grown on Ge (001) substrate.*

by fitting are plotted in Figure 10. The modeled spectra and the experimental data are in good agreement with each other (Figure S4e-h).

In Figure 10a, a rise in growth temperature from 20 °C to 250 °C leads to a decrease in scattering rate from 2.7 to 1.3 × 10^{14} rad/s. At 300 °C, the scattering rate remains unchanged at 1.3 × 10^{14} rad/s. Figure 10b also shows that as growth temperature increases, plasma wavelength increases from 4.0 to 5.3 μm. We can understand this trend in much the same way as the inverse relationship between carrier concentration and electrical mobility. Yet, the epitaxial character of the films on Ge compared to the polycrystalline films on Si does not result in reduced carrier scattering determined from fits to the reflectance. This supports the underlying hypothesis that crystal defects are not the dominant scattering centers in SnTe. While the surface roughness is indeed appropriate for subsequent device integration, we need to explore further routes to single crystal films in future work. These include the

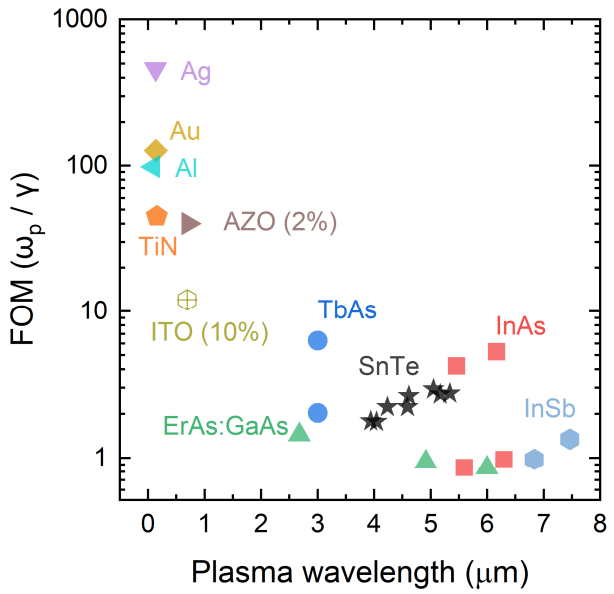

Figure 11. *Comparison of figure-of-merit (FOM) of SnTe with other plasmonic materials (Ag, Au, Al, TiN, AZO, ITO*[45,46]*, ErAs:GasAs*[12]*, TbAs*[13]*, InSb*[7]*, and InAs*[5,15,16]

use of a substrate offcut or different chemical and thermal methods to prepare the Ge surface prior to SnTe deposition.

Finally, we compare SnTe with other plasmonic materials using the figure-of-merit defined as the ratio of the plasma frequency ω_p and the materials loss γ.[45,47] Figure 11 shows this for our sputtered SnTe films and we find it comparable to that of doped MBE-grown III-V semiconductors in the mid-IR. At a plasma wavelength of approximately 5.3 μm, the deposited SnTe films have comparable loss to InAs. We include two sets of reported results for InAs with different material loss as this property appears to be sensitive to MBE growth parameters. On the other hand, we find our polycrystalline SnTe films comparable in loss to single crystal bulk materials. This result highlights the potential of SnTe as a mid-IR plasmonic material that can be synthesized using non-UHV methods. In addition to

achieving epitaxy, future work will focus on extrinsic doping via sputtering, including counter-doping of the Sn vacancies, to expand the wavelength tunability of this system.

SUMMARY AND CONCLUSIONS

In conclusion, we grow SnTe films on CMOS-compatible substrates of Si and Ge substrates using RF sputtering. While sputtered SnTe films on Si (001) are polycrystalline and have high surface roughness, growth on Ge (001) films yield smoother films with better crystallinity, making it more suitable device fabrication. In the latter case, SnTe films have two sets of epitaxial grains differing only in their in-plane orientation to Ge – a majority being cube-on-cube and a minority being 45° rotated in-plane. Despite not being single crystalline, SnTe films with carrier concentrations between 10^{20} – 10^{21} cm^{-3} exhibit mobility that is almost half that of high-quality bulk crystals. They host comparable optical scattering loss to heavily doped narrow bandgap III-V plasmonic materials and have tunable plasma wavelength in the range of 3.9 to 5.3 μm using SnTe nonstoichiometry alone. Future work will be geared towards achieving fully cube-on-cube epitaxial films on Ge, as well as exploring extrinsic dopants to increase the range of plasma wavelength tunability.

ASSOCIATED CONTENT

Supporting information

Additional details on DC sputtering growth of SnTe films (Figure S1), the effect of thicker films on hole concentration (Figure S2), re-scaled AFM scans of films on Ge (Figure S3), and reflection fitting of SnTe films (Figure S4). (PDF)

AUTHOR INFORMATION

Corresponding Author

***Email:** kunalm@stanford.edu

Notes

The authors have no conflicts to disclose.

ACKNOWLEDGMENTS

We gratefully acknowledge support via NSF CAREER award under Grant No. DMR-2036520. Part of this work was performed at the Stanford Nanofabrication Facilities (SNF) and Stanford Nano Shared Facilities (SNSF), supported by the National Science Foundation under award ECCS-2026822.

REFERENCES

(1) Poddubny, A.; Iorsh, I.; Belov, P.; Kivshar, Y. Hyperbolic Metamaterials. *Nature Photon* **2013**, *7* (12), 948–957. 10.1038/nphoton.2013.243.

(2) Smith, D. R.; Schurig, D.; Mock, J. J.; Kolinko, P.; Rye, P. Partial Focusing of Radiation by a Slab of Indefinite Media. *Applied Physics Letters* **2004**, *84* (13), 2244–2246. 10.1063/1.1690471.

(3) Shalaev, V. M. Transforming Light. *Science* **2008**, *322* (5900), 384–386. 10.1126/science.1166079.

(4) Homola, J. Surface Plasmon Resonance Sensors for Detection of Chemical and Biological Species. *Chem. Rev.* **2008**, *108* (2), 462–493. 10.1021/cr068107d.

(5) Law, S.; Adams, D. C.; Taylor, A. M.; Wasserman, D. Mid-Infrared Designer Metals. *Optica Express* **2012**, *20*, 12155–12165.

(6) N'Tsame Guilengui, V.; Cerutti, L.; Rodriguez, J.-B.; Tournié, E.; Taliercio, T. Localized Surface Plasmon Resonances in Highly Doped Semiconductors Nanostructures. *Applied Physics Letters* **2012**, *101* (16), 161113. 10.1063/1.4760281.

(7) Law, S.; Liu, R.; Wasserman, D. Doped Semiconductors with Band-Edge Plasma Frequencies. *Journal of Vacuum Science & Technology B* **2014**, *32* (5), 052601. 10.1116/1.4891170.

(8) Baldassarre, L.; Sakat, E.; Frigerio, J.; Samarelli, A.; Gallacher, K.; Calandrini, E.; Isella, G.; Paul, D. J.; Ortolani, M.; Biagioni, P. Midinfrared Plasmon-Enhanced Spectroscopy with Germanium Antennas on Silicon Substrates. *Nano Lett.* **2015**, *15* (11), 7225–7231. 10.1021/acs.nanolett.5b03247.

(9) Frigerio, J.; Ballabio, A.; Isella, G.; Sakat, E.; Pellegrini, G.; Biagioni, P.; Bollani, M.; Napolitani, E.; Manganelli, C.; Virgilio, M.; Grupp, A.; Fischer, M. P.; Brida, D.; Gallacher, K.; Paul, D. J.; Baldassarre, L.; Calvani, P.; Giliberti, V.; Nucara, A.; Ortolani, M. Tunability of the Dielectric Function of Heavily Doped Germanium Thin Films for Mid-Infrared Plasmonics. *Phys. Rev. B* **2016**, *94* (8), 085202. 10.1103/PhysRevB.94.085202.

(10) Barho, F. B.; Gonzalez-Posada, F.; Milla-Rodrigo, M.-J.; Bomers, M.; Cerutti, L.; Taliercio, T. All-Semiconductor Plasmonic Gratings for Biosensing Applications in the Mid-Infrared Spectral Range. *Opt. Express* **2016**, *24* (14), 16175–16190. 10.1364/OE.24.016175.

(11) Dong, Z.; Vinnakota, R. K.; Briggs, A. F.; Nordin, L.; Bank, S. R.; Genov, D. A.; Wasserman, D. Electrical Modulation of Degenerate Semiconductor Plasmonic Interfaces. *Journal of Applied Physics* **2019**, *126* (4), 043101. 10.1063/1.5108905.

(12) Wang, Y.; Wei, D.; Sohr, P.; Zide, J. M. O.; Law, S. Extending the Tunable Plasma Wavelength in III–V Semiconductors from the Mid-Infrared to the Short-Wave Infrared by Embedding Self-Assembled ErAs Nanostructures in GaAs. *Advanced Optical Materials* **2020**, *8* (7), 1900937. 10.1002/adom.201900937.

(13) Wang, Y.; Bork, J.; Law, S.; Zide, J. M. O. Improved Epitaxial Growth of TbAs Film on III–V Semiconductors. *Journal of Vacuum Science & Technology A* **2020**, *38* (3), 033405. 10.1116/1.5144999.

(14) Nordin, L.; Wasserman, D. Epitaxial Mid-IR Nanophotonic Optoelectronics. *Applied Physics Letters* **2022**, *120* (22), 220501. 10.1063/5.0086774.

(15) Wei, D.; Maddox, S.; Sohr, P.; Bank, S.; Law, S. Enlarged Growth Window for Plasmonic Silicon-Doped InAs Using a Bismuth Surfactant. *Opt. Mater. Express* **2020**, *10* (2), 302–311. 10.1364/OME.383260.
(16) Law, S.; Yu, L.; Wasserman, D. Epitaxial Growth of Engineered Metals for Mid-Infrared Plasmonics. *Journal of Vacuum Science & Technology B* **2013**, *31* (3), 03C121. 10.1116/1.4797487.
(17) Rogers, L. M. Valence Band Structure of SnTe. *J. Phys. D: Appl. Phys.* **1968**, *1* (7), 845. 10.1088/0022-3727/1/7/304.
(18) Wang, N.; West, D.; Liu, J.; Li, J.; Yan, Q.; Gu, B.-L.; Zhang, S. B.; Duan, W. Microscopic Origin of the p -Type Conductivity of the Topological Crystalline Insulator SnTe and the Effect of Pb Alloying. *Phys. Rev. B* **2014**, *89* (4), 045142. 10.1103/PhysRevB.89.045142.
(19) Brebrick, R. F. Deviations from Stoichiometry and Electrical Properties in SnTe. *Journal of Physics and Chemistry of Solids* **1963**, *24* (1), 27–36. 10.1016/0022-3697(63)90038-6.
(20) Bis, R. F.; Dixon, J. R. Electric-Susceptibility Mass of Free Holes in SnTe. *Phys. Rev. B* **1970**, *2* (4), 1004–1012. 10.1103/PhysRevB.2.1004.
(21) Riedl, H. R.; Dixon, J. R.; Schoolar, R. B. Reflectivity of Tin Telluride in the Infrared. *Phys. Rev.* **1967**, *162* (3), 692–700. 10.1103/PhysRev.162.692.
(22) Burke, J. R.; Riedl, H. R. Temperature Dependence of the Optical Absorption Edge of p -Type SnTe. *Phys. Rev.* **1969**, *184* (3), 830–836. 10.1103/PhysRev.184.830.
(23) Tsu, R.; Howard, W. E.; Esaki, L. Optical and Electrical Properties and Band Structure of GeTe and SnTe. *Phys. Rev.* **1968**, *172* (3), 779–788. 10.1103/PhysRev.172.779.
(24) Liu, H.; Liu, Y.; Dong, S.; Xu, H.; Wu, Y.; Hao, L.; Cao, B.; Li, M.; Wang, Z.; Han, Z.; Yan, K. Photothermoelectric SnTe Photodetector with Broad Spectral Response and High On/Off Ratio. *ACS Appl. Mater. Interfaces* **2020**, *12* (44), 49830–49839. 10.1021/acsami.0c15639.
(25) Klett, R.; Schönle, J.; Becker, A.; Dyck, D.; Borisov, K.; Rott, K.; Ramermann, D.; Büker, B.; Haskenhoff, J.; Krieft, J.; Hübner, T.; Reimer, O.; Shekhar, C.; Schmalhorst, J.-M.; Hütten, A.; Felser, C.; Wernsdorfer, W.; Reiss, G. Proximity-Induced Superconductivity and Quantum Interference in Topological Crystalline Insulator SnTe Thin-Film Devices. *Nano Lett.* **2018**, *18* (2), 1264–1268. 10.1021/acs.nanolett.7b04870.
(26) Song, L.; Tang, L.; Hao, Q.; Teng, K. S.; Lv, H.; Wang, J.; Feng, J.; Zhou, Y.; He, W.; Wang, W. Broadband Photodetector Based on SnTe Nanofilm/n-Ge Heterostructure. *Nanotechnology* **2022**, *33* (42), 425203. 10.1088/1361-6528/ac80cc.
(27) Zhong, A.; Zhou, Y.; Jin, H.; Yu, H.; Wang, Y.; Luo, J.; Huang, L.; Sun, Z.; Zhang, D.; Fan, P. Superior Performances of Self-Driven Near-Infrared Photodetectors Based on the SnTe:Si/Si Heterostructure Boosted by Bulk Photovoltaic Effect. *Small* **2023**, *19* (14), 2206262. 10.1002/smll.202206262.
23. Suzuki, N. & Adachi, S. Optical Properties of SnTe. *Jpn. J. Appl. Phys.* **34**, 5977 (1995).
(29) Madiomanana, K.; Bahri, M.; Rodriguez, J. B.; Largeau, L.; Cerutti, L.; Mauguin, O.; Castellano, A.; Patriarche, G.; Tournié, E. Silicon Surface Preparation for III-V

Molecular Beam Epitaxy. *Journal of Crystal Growth* **2015**, *413*, 17–24. 10.1016/j.jcrysgro.2014.12.004.
(30) Carroll, M. S.; Sturm, J. C.; Yang, M. Low-Temperature Preparation of Oxygen- and Carbon-Free Silicon and Silicon-Germanium Surfaces for Silicon and Silicon-Germanium Epitaxial Growth by Rapid Thermal Chemical Vapor Deposition. *J. Electrochem. Soc.* **2000**, *147* (12), 4652. 10.1149/1.1394118.
(31) Zhou, M.; Gibbs, Z. M.; Wang, H.; Han, Y.; Xin, C.; Li, L.; Snyder, G. J. Optimization of Thermoelectric Efficiency in SnTe: The Case for the Light Band. *Phys. Chem. Chem. Phys.* **2014**, *16* (38), 20741–20748. 10.1039/C4CP02091J.
(32) Li, S.; Xin, J.; Li, W.; Tao, Y.; Xu, T.; Xiao, B.; Luo, Y.; Jiang, Q.; Yang, J. Enhanced Thermoelectric Performance of Orientated and Defected SnTe. *Journal of Alloys and Compounds* **2021**, *858*, 157634. 10.1016/j.jallcom.2020.157634.
(33) Hua, F.; Lv, P.; Hong, M.; Xie, S.; Zhang, M.; Zhang, C.; Wang, W.; Wang, Z.; Liu, Y.; Yan, Y.; Yuan, S.; Liu, W.; Tang, X. Native Atomic Defects Manipulation for Enhancing the Electronic Transport Properties of Epitaxial SnTe Films. *ACS Appl. Mater. Interfaces* **2021**, *13* (47), 56446–56455. 10.1021/acsami.1c15447.
(34) Xu, S.; Zhu, W.; Zhao, H.; Xu, L.; Sheng, P.; Zhao, G.; Deng, Y. Enhanced Thermoelectric Performance of SnTe Thin Film through Designing Oriented Nanopillar Structure. *Journal of Alloys and Compounds* **2018**, *737*, 167–173. 10.1016/j.jallcom.2017.12.011.
(35) Assaf, B. A.; Katmis, F.; Wei, P.; Satpati, B.; Zhang, Z.; Bennett, S. P.; Harris, V. G.; Moodera, J. S.; Heiman, D. Quantum Coherent Transport in SnTe Topological Crystalline Insulator Thin Films. *Applied Physics Letters* **2014**, *105* (10), 102108. 10.1063/1.4895456.
(36) Toneva, A.; Alazhazhian, A. Mobility in P-Pb1−xSnxTe. *physica status solidi (a)* **1977**, *44* (2), 621–626. 10.1002/pssa.2210440226.
(37) Corsi, C.; Fainelli, E.; Petrocco, G.; Vitali, G.; Campisano, U.; Foti, G.; Rimini, E. Single-Crystal Heteroepitaxial Growth of Pbsnte Films on Germanium Substrates by r.f. Sputtering. *Thin Solid Films* **1976**, *33*, 135–148.
(38) McDowell, L. L.; Qiu, J.; Mirzaei, M. R.; Weng, B.; Shi, Z. Integration of Epitaxial IV–VI Pb-Chalcogenide on Group IV Vicinal Ge Substrate to Form p–n Heterogeneous Structures. *Crystal Growth & Design* **2022**, *22* (1), 461–468. 10.1021/acs.cgd.1c01074.
(39) Ponath, P.; Posadas, A. B.; Demkov, A. A. Ge(001) Surface Cleaning Methods for Device Integration. *Applied Physics Reviews* **2017**, *4* (2), 021308. 10.1063/1.4984975.
(40) Kita, K.; Takahashi, T.; Nomura, H.; Suzuki, S.; Nishimura, T.; Toriumi, A. Control of High-k/Germanium Interface Properties through Selection of High-k Materials and Suppression of GeO Volatilization. *Applied Surface Science* **2008**, *254* (19), 6100–6105. 10.1016/j.apsusc.2008.02.158.
(41) Prabhakaran, K.; Maeda, F.; Watanabe, Y.; Ogino, T. Distinctly Different Thermal Decomposition Pathways of Ultrathin Oxide Layer on Ge and Si Surfaces. *Applied Physics Letters* **2000**, *76* (16), 2244–2246. 10.1063/1.126309.
(42) Toriumi, A.; Tabata, T.; Hyun Lee, C.; Nishimura, T.; Kita, K.; Nagashio, K. Opportunities and Challenges for Ge CMOS – Control of Interfacing Field on Ge Is

a Key (Invited Paper). *Microelectronic Engineering* **2009**, *86* (7), 1571–1576. 10.1016/j.mee.2009.03.052.
(43) Prabhakaran, K.; Ogino, T. Oxidation of Ge(100) and Ge(111) Surfaces: An UPS and XPS Study. *Surface Science* **1995**, *325* (3), 263–271. 10.1016/0039-6028(94)00746-2.
(44) Zhang, X.-J.; Xue, G.; Agarwal, A.; Tsu, R.; Hasan, M.-A.; Greene, J. E.; Rockett, A. Thermal Desorption of Ultraviolet–Ozone Oxidized Ge(001) for Substrate Cleaning. *Journal of Vacuum Science & Technology A: Vacuum, Surfaces, and Films* **1993**, *11* (5), 2553–2561. 10.1116/1.578606.
(45) Khurgin, J. B. Replacing Noble Metals with Alternative Materials in Plasmonics and Metamaterials: How Good an Idea? *Philosophical Transactions of the Royal Society A: Mathematical, Physical and Engineering Sciences* **2017**, *375* (2090), 20160068. 10.1098/rsta.2016.0068.
(46) Naik, G. V.; Shalaev, V. M.; Boltasseva, A. Alternative Plasmonic Materials: Beyond Gold and Silver. *Advanced Materials* **2013**, *25* (24), 3264–3294. 10.1002/adma.201205076.
(47) Hsieh, W. T.; Wu, P. C.; Khurgin, J. B.; Tsai, D. P.; Liu, N.; Sun, G. Comparative Analysis of Metals and Alternative Infrared Plasmonic Materials. *ACS Photonics* **2018**, *5* (7), 2541–2548. 10.1021/acsphotonics.7b01166.

Supporting Information

Sputtered SnTe thin films on Si and Ge as a plasmonic material

Tri Nguyen[1], Leland Nordin[2], Kunal Mukherjee[1]

[1]Materials Science and Engineering, Stanford University, CA 94305, United States

[2]Geballe Laboratory for Advanced Materials, Stanford University, CA 94305, United States

A. DC sputtered growth of SnTe-on-Ge(001)

Here we reported preliminary structural and optical characterization of SnTe film deposited on Ge (001) at a substrate temperature of 250 °C, using Ar flow of 50 sccm, chamber pressure of 3mTorr, and sputtering power of 60W DC. The native oxides of Ge were removed by baking at 650 °C for an hour under high-vacuum before deposition. After deposition, the DC sputtered film has cracks with widths ranging between 50 - 200 μm due to thermal stress, but the structural and optical properties are comparable to those of RF sputtered film. Figure S1a shows the atomic force microscopy (AFM) of SnTe films, showing morphologies characteristic of epitaxial films with a sub-nanometer surface roughness of 0.4 nm. A symmetric 2θ/ω scan of the SnTe/Ge (001) films in Figure S1b shows the films grew single-orientation out-of-plane. Figure S1c shows the 360º phi scans on the {224} peaks of SnTe and Ge, revealing two sets of epitaxial domain grains: a majority being cube-on-cube and a minority being 45º rotated in-plane. Figure S1d shows the reflection spectrum of SnTe films. We fit the data and obtain a plasma wavelength of 4.7 μm, a scattering rate of 1.6×10^{14} rad/s, and a thickness of 1.28 μm, which is ~3.7 times

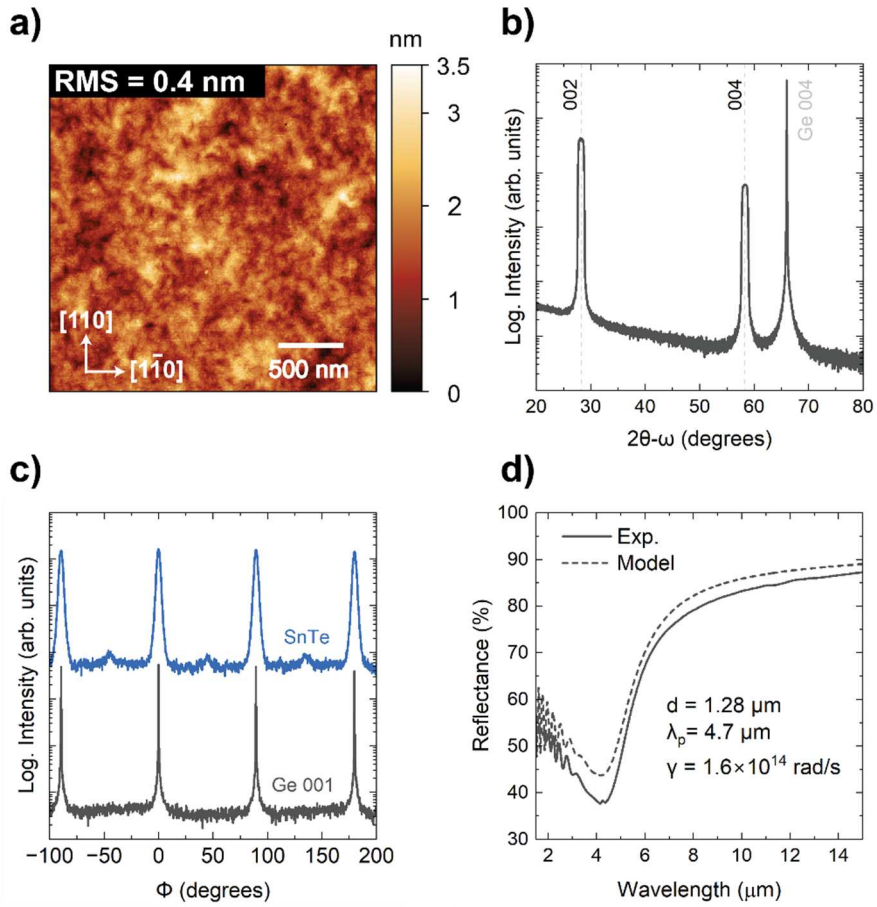

Figure S1: *(a) AFM topography map, (b) Symmetric 2θ/ω scan, (c) 360⁰ phi scans showing SnTe and Ge {224}at χ = 35.26⁰, and (d) Reflectance spectrum of SnTe/Ge(001) deposited at 250 ℃ using DC sputtering magnetron source.*

thicker than that of SnTe films deposited using RF under the similar conditions. The result highlights the versatility of SnTe films to be sputtered using either RF or DC sources.

B. Effect of thickness on carrier concentration

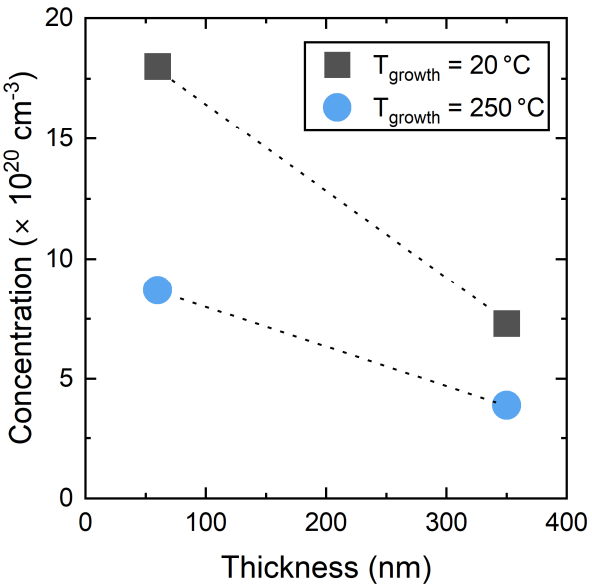

Figure S2: *Hole concentration of SnTe films grown on Si (001) versus film thickness at growth temperatures of 20 ℃ and 250 ℃.*

Here we plot a subset of the SnTe-on-Si(001) films, showing the effect of thickness on hole concentration for two different growth temperatures. Supplementary Figure S2 shows that in both cases, as the film thickness increases from 60 nm to 350 nm, the hole concentration is reduced approximately by a factor of two. This result hints at a potential interfacial connection to free carrier concentration, but we do not investigate this further.

C. Film morphology on Ge

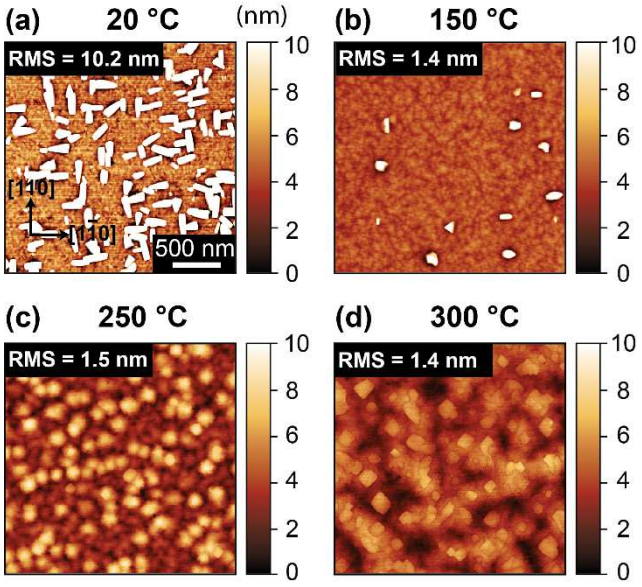

Figure S3. *AFM topography maps of SnTe films on Ge (001) deposited at (a) 20 ℃, (b) 150 ℃, (c) 250 ℃, and (d) 300 ℃ shown also as Fig. 7. The scan area is 2.5 x 2.5 μm^2.The height scale is enhanced to show the very smooth films at 20 °C and 150 °C in between the prominent grains.*

D. Additional reflection fitting

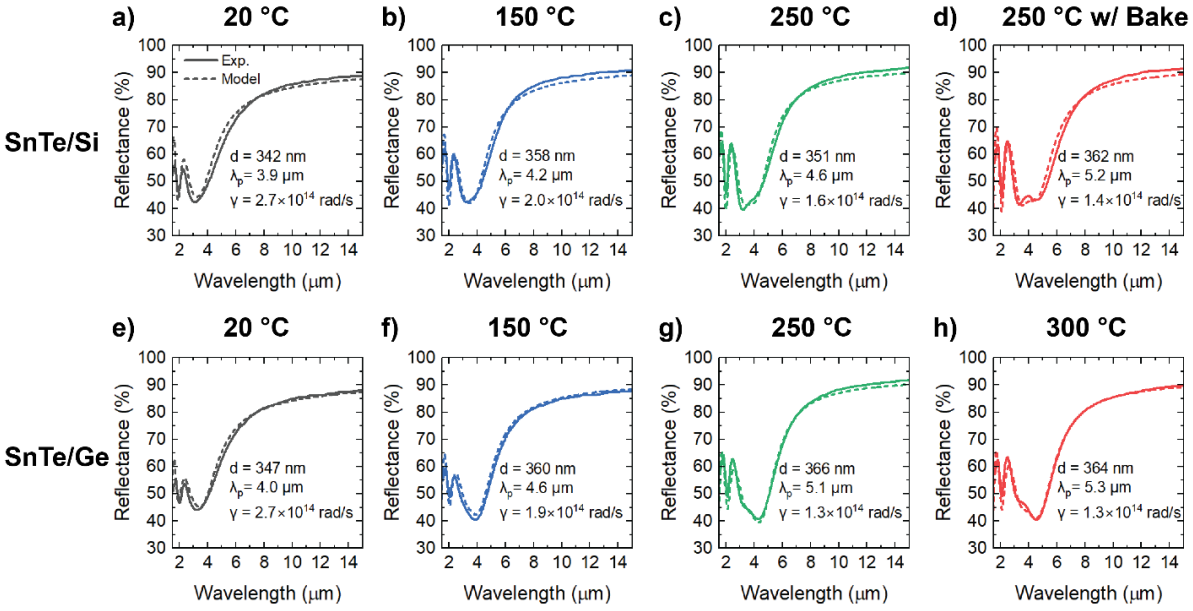

Figure S3: *Experimental (solid lines) and modeled (dashed lines) reflection for SnTe films grown on Si (001) using a substrate temperature of (a) 20 ℃, (b) 150 ℃, (c) 250 ℃, and (d) 250 ℃ with a pre-deposition substrate bake at 650℃ for an hour, and for SnTe films grown on Ge (001) using a substrate temperature of (e) 20 ℃, (f) 150 ℃, (g) 250 ℃, and (h) 300 ℃. The fitting parameters used for the modelling (thickness d, plasma wavelength λ_p, and scattering rate γ) are given in the lower right-hand corner of each figure.*

Reflection data of SnTe films grown on Si (001) and Ge (001) are fitted using the 3-layer transfer-matrix combined with the Drude model as described in the Methods section. Supplementary Figure S4 shows good qualitative agreement between the experimental and modeled spectra. The three fitting parameters used for the modelling (films thickness d, plasma wavelength λ_p, and scattering rate γ) are listed in the lower right corner of each figure.